Hanau, Germany. Small neodymium–iron–boron magnets, available from Edmund Scientific and elsewhere, appear to be a reasonable alternative.

[2] How closely a simple dipole approximates the field of a cylindrical magnet can be estimated numerically. The conclusions depend, as may well be imagined, on the ratio of diameter to length of the magnet, on azimuthal angle, and, most importantly, on the distance from the center of the magnet. In all quantitative measurements reported in this paper, the dipole approximation is accurate to 5% or better.

[3] W. J. Duffin, *Electricity and Magnetism* (McGraw-Hill, Maidenhead, Berkshire, UK 1980), 3rd ed.

[4] Reference 3, pp. 197–199.

[5] Reference 3, pp. 333–334.

[6] E. W. Lee, in *Encyclopaedic Dictionary of Physics*, edited by J. Thewlis (Pergamon, Oxford, UK 1961), Vol. 4, pp. 474–476.

[7] R. Stuart Mackay, "Two startling demonstrations with a magnet," Am. J. Phys. **28**, 678 (1960).

[8] T. J. Quinn, C. C. Speake, and R. S. Davis, "A 1 kg mass comparator using flexure-strip suspension: Preliminary results," Metrologia **23**, 87–100 (1986/87).

[9] C. C. Speake and T. J. Quinn, "Search for a short-range, isospin-coupling component of the fifth force with use of a beam balance," Phys. Rev. Lett. **61**, 1340–1343 (1988).

[10] Although we define and use the term susceptibility, we have deliberately not introduced a symbol for this quantity. Relative permeability μ_r in the SI may be directly compared with permeability in the cgs system. As for comparisons of susceptibility, the opportunities for confusion are plentiful.

[11] J. D. Jackson, *Classical Electrodynamics* (Wiley, New York, 1975), 2nd ed., p. 207 (problem 5.10).

[12] It is interesting to verify that results of comparable accuracy can be obtained using dipole images: Replace S in Fig. 3 by a cylindrical slab of mild steel. A semi-infinite slab would attract M with the same force (nearly) as that due to an image magnet, identical to M, placed coaxially at a distance $2z_0$; Eq. (4) is thus appropriate. (Make $R \gg 2z_0$ to approximate infinite radius. Subtract the force due to a magnet located at $2z_1$ to correct for finite thickness.)

[13] These materials also have a relatively limited region of linearity: For similar samples placed in a uniform **B** field, $\mu_r - 1$ was found to fall by an order of magnitude as the field increased from 2 to 100 mT (20 to 1000 G). I am indebted to Anthony Drake of the National Physical Laboratory, Teddington, UK for these measurements.

[14] F. A. Gould, "Tests of highly non-magnetic stainless steels for use in the construction of weights," J. Sci. Instrum. **23**, 124–127 (1946).

[15] S. S. Eaton and G. R. Eaton, "An inexpensive, convenient demonstration of magnetic susceptibility," J. Chem. Educ. **56**, 170–171 (1979).

[16] In practice, we need not concern ourselves with forces that remain constant during weighing operations but only those that are synchronous with the changing of masses on the balance pan. There are, of course, other sources of magnetic interaction which have been ignored in this paper, e.g., changes in ambient fields and their gradients.

[17] Reference 3, p. 343.

The electronic bouncing ball

Robert L. Zimmerman
FFCLRP-USP, 14100, Ribeirão Preto, São Paulo, Brazil

Sergio Celaschi
CPqD-Telebrás, 13085, Campinas, São Paulo, Brazil

Luis G. Neto
IFQSC-USP, 13560, São Carlos, São Paulo, Brazil

(Received 10 April 1991; accepted 27 August 1991)

The electronic analog of the bouncing ball is developed as a simple classroom experiment illustrating all the important features of this nonlinear chaotic system. In an operational amplifier circuit conventionally used to simulate the free fall of a ball in constant gravity, current feedback through a precision diode rectifier is used to model free fall when the rectifier is backward biased, and the bounce when the rectifier is conducting. The ease with which parameters are controlled and variables measured permits the investigation in great detail of the specific dynamic behavior of the bouncing ball.

I. INTRODUCTION

Many dynamical problems cannot be analytically solved. Simple Hamiltonian or dissipative systems governed by a few dynamical variables and characterized by a few parameters may belong to this class. The main reason for this difficulty lies in the fact that such systems, governed by regular differential equations, may behave erratically in time. During recent years, this erratic or chaotic behavior has been the focus of attention due to its inherent beauty.[1,2] One apparently simple dynamic system that exhibits remarkably complex behavior is the bouncing ball. First introduced by Fermi,[3] and more recently studied experimentally and theoretically by many others,[4–7] the bouncing ball is a one-variable, two-parameter system governed by Newton's equation. A complete correlation between theory and experiment has been obtained for this system. Experimentally, the system consists of a ball bouncing vertically, under gravity, on a harmonically vibrating surface. The two control parameters are the dissipation, which may be characterized by a coefficient of restitution K for the impacts, and the ratio α between the acceleration due to the vibrating surface and that due to gravity. This simple one-dimensional mechanical system

has been used as an undergraduate experiment to illustrate the evolution of a well-behaved dynamic system toward chaos.[6] Although the bouncing ball is unique in its simplicity of conception and complexity of its behavior, the mechanical experiment has some major drawbacks. First, the period doubling routes, due to noise, are restricted to the first subharmonic bifurcation.[6,7] Second, the experimental setup for the bouncing ball requires complex electronic equipment to explore the strange attractors that arise from the chaotic motions.[8]

In this paper, we introduce an electronic analog of the mechanical bouncing ball by use of an elementary circuit composed of three operational amplifiers with feedback current from a rectifier. Since all signals are electrical, data collection and analysis become quite simple. Unlike previous mechanical experiments in which the coefficient of restitution was fixed, this electrical analog allows the student to explore experimentally an ample region of the parameter space of the system. Most of the features of a nonlinear systems, namely multiple period doubling bifurcations, strange attractors, crisis, fractal dimension, and intermittancy are accessible to undergraduate students by use of an oscilloscope.

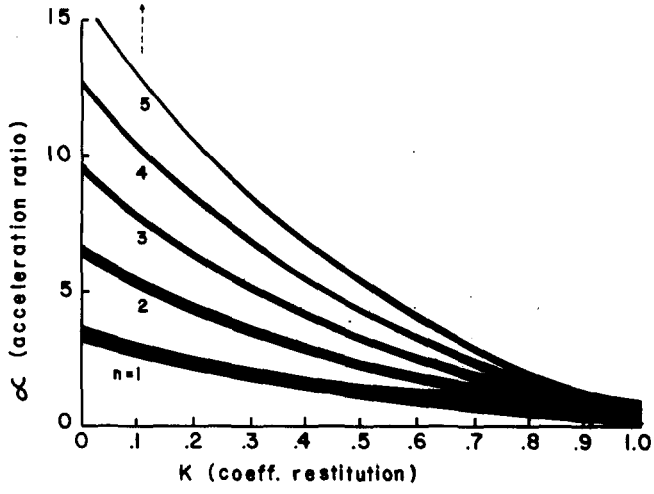

Fig. 1. Two-dimensional parameter space for the bouncing ball showing the range of stability of simple orbits according to Eq. (4).

II. THE BOUNCING BALL

The ball leaves the vibrating table, after the Nth impact, with velocity v_N when the table phase is Φ_N, and contacts the table after a time t_N, governed by the equation

$$x_{0T}\sin\Phi_N + v_N t_N - gt_N^2/2 = x_{0T}\sin(\omega t_N + \Phi_N), \tag{1}$$

where g is the gravitational constant, x_{0T} and ω are the amplitude and angular frequency of the table, respectively. For the next trajectory, immediately after the $(N+1)$th impact, the table phase Φ_{N+1} and the new departure velocity are determined from the coupled parametric recursion relations

$$\Phi_{N+1} = \Phi_N + \omega t_N, \tag{2}$$

$$v_{N+1} = K(gt_N - v_N) + x_{0T}\omega(1+K)(\Phi_N + \omega t_N). \tag{3}$$

Equation (3) defines the coefficient of instantaneous restitution K.[4] After normalization,[6] the set of Eqs. (1)–(3) reveals that the dynamics of this system is governed by only two parameters; K and $\alpha \equiv \omega^2 x_{0T}/g$; the normalized table acceleration. For a given set of parameters (K and α), Eqs. (2) and (3) are iterated from selected initial conditions until a limit cycle is found or until a chaotic regime is characterized by its strange attractor.

In 1975, Pippard[4] noticed that, for a fixed K, there are ranges of values for the parameter α that give stable orbits with periodic impacts at n times the period of the table, $2n$ times that period, and other subharmonics. He derived an expression for these ranges of stability:

$$\alpha_n^{\text{saddle/node}} < \alpha_n < \alpha_n^{\text{saddle/node}} \times\{1 + [2(1+K^2)/n\pi(1-K^2)]^2\}^{1/2}, \tag{4}$$

where

$$\alpha_n^{\text{saddle/node}} = n\pi(1-K)/(1+K).$$

These relations are displayed graphically in Fig. 1 for the first five values of n, the number of tables cycles per impact. In the above equalities, $0<K<1$ is the coefficient of restitution. The upper limits for each n value are critical values beyond which subharmonic orbits may be stable, the period doubling. After the discovery of the universal nature of the period-doubling route to chaos in nonlinear systems in general, details about the subharmonic limit cycles and about the chaotic movements that exist beyond Pippard's upper limit were published.[6–9] Indeed, for the extremely dissipative case, the bifurcation diagram for the bouncing ball for each n number resembles that for the logistic equation.[1] According to Eq. (4), the upper limit of stability of the first orbit ($n=1$) overlaps with the lower limit of stability for the next higher orbit($n=2$) for values of the coefficient of restitution above $K_c = 0.6800$. Then, for $K > K_c$ various limit cycles and chaotic movements may be reached at fixed values of K and α merely by changing the initial conditions.

It is not necessary to discuss in this article more details on the dynamics of the bouncing ball. These details have been observed in the mechanical experiment and from numerical simulation.[6] Suffice it to say that our electronic analog permits a student to display on an oscilloscope or a strip-chart recorder all the dynamics of the ideal physical system, as well as some important additional abstract concepts not easily observable in the mechanical experiment. In the following section the analogy between the mechanical and the electronic systems is established. Techniques for obtaining the oscilloscope displays are described in detail, and some of the results are presented.

III. ESTABLISHING THE ANALOGY

The electronic analog of the mechanical bouncing ball is shown schematically in Fig. 2. The three operational amplifiers are JFET linear differential amplifiers with open loop gain of about 25 000. The inset shows an optional precision diode rectifier circuit that may be used to idealize the characteristic of the feedback diode. This precision rectifier (the "diode") ensures that the feedback current to the summing point S_1 is controlled by linear elements. No voltage or current offset corrective circuits are necessary. The

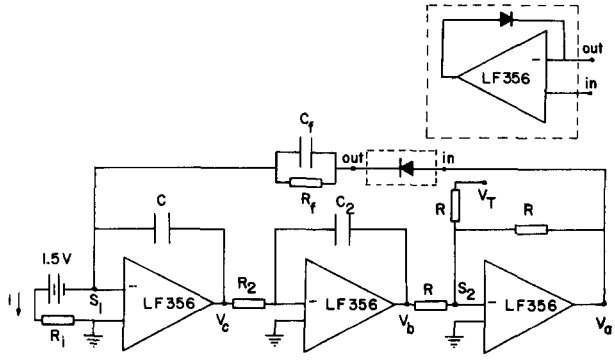

Fig. 2. Circuit diagram. Inset—precision rectifier that may be substituted for the diode.

components are mounted with no electrostatic shielding on a circuit board supplied with bipolar dc voltage from common sources. All $C = 0.047$ μF except for C_f, and all $R = 10$ kΩ except R_f, and $R_i = 1$ MΩ. Voltages may be selected for oscilloscope display of the position of the ball (V_b), position of the table ($-V_T$), or the velocity of the ball ($-V_c$).

We show in this section that the electronic analog simulates free fall when the "diode" is reverse biased, and impact when it conducts. During impact with the table, the ball experiences a force opposite to and much larger than the gravitational force acting on it during free fall. The circuit also simulates a third regime, with $\alpha = (1-K)/(1+K)$, during which the ball must come to maintain permanent contact with the table.

A. Free fall

When the "diode" is reverse biased, the current i, leaving the summing point S_1 (Fig. 2) of the first operational amplifier, causes the charge Q and the voltage V_c on the capacitance C to change according to

$$i = C\frac{dV_c}{dt} \quad \text{(Amp)}. \tag{5}$$

To simulate the negative gravitational force, the current is directed as shown in Fig. 2. The second and third operational amplifiers, an integrator and a gain-one inverter, respectively, produce an output voltage V_a given by

$$R_2C_2V_a(t) = \int V_c(t')dt' \ \text{(V s)}. \tag{6}$$

When the "diode" is reverse biased, and the current i is much larger than the intrinsic "diode" reverse current, Eqs. (5) and (6) can be written in the familiar second-order differential form

$$R_2C_2\frac{d^2V_a}{dt^2} = \frac{i}{C}, \tag{7}$$

which is analogous to

$$\frac{d^2x}{dt^2} = g. \tag{8}$$

Thus for negative constant current i, the parabolic solution of Eq. (7) describes the analogy to the time dependent position x of a freely falling mass in a constant gravitational field g. This circuit, without feedback, has been used long ago for analog computation in ballistics to determine the time and position of impact of a projectile on a target.

B. Impact

When the "diode" is conducting, it limits the parabolic excursion by providing a large current that exactly inverts the voltage on the capacitance C in a time too short to alter the charge on C_2. Thus V_c inverts at a fixed V_a which is analogous to the inversion of the velocity during a perfectly elastic impact of a rigid ball on a table at a fixed position. Without dissipative elements in the feedback loop, impact and parabolic free fall repeat endlessly, as though the coefficient of restitution were unity. A resistance R_f in series with the precision rectifier limits the feedback current and represents an increase of the contact time between the ball and the table. The parabolas then become joined by one-half cycle of a sine-like function, exactly replicating a perfectly elastic impact between the ball and the table, where one or both are deformable. The time interval of contact π/ω_0 is

$$\pi/\omega_0 = (R_fCR_2C_2)^{1/2}, \tag{9}$$

where ω_0 is the natural frequency of the circuit considering just the R_f impedance in the feedback loop. For $R_f = 0$, the duration of contact does not vanish. Instead, it is controlled by the forward dynamic resistance of the rectifier. In mechanical experiments, the position of the table is varied harmonically in time to furnish energy to the bouncing ball. Analogously, a varying voltage $V_T(t) = V_{0T}\cos(\omega t)$, added to the output V_a at S_2 (Fig. 2), furnishes energy to the circuit and modifies Eq. (6). Dissipation during contact is accomplished by a capacitance C_f in parallel with R_f (in series with the feedback rectifier). The excursions remain perfectly parabolic but the half-sine cycle during contact shows a phase shift and damping as though the coefficient of restitution were less than unity. Thus the circuit has analogs to all the aspects of the ball bouncing on a vibrating table; namely, free fall, dissipative or elastic impacts, and energy exchange with the movable table. During the contact time interval when V_a becomes positive, the precision rectifier conducts in a direction opposite to the current i used to simulate the downward gravitational force. Equations (6) and (7) then become

$$C\frac{dV_c}{dt} = -\frac{V_a}{R_f} - C_f\frac{dV_a}{dt} - i, \tag{10}$$

$$R_2C_2V_a(t) = \int V_c(t')\cdot dt' - R_2C_2V_T(t). \tag{11}$$

While V_c is still the analog of the ball velocity, $V_a(t)$ and dV_a/dt are, respectively, the analogs of position and velocity of the ball relative to the table. Substituting Eq. (11) into (10), gives the equation of motion, valid during contact, which is that of a damped linear oscillator:

$$\frac{dV_c}{dt} + \frac{V_c}{\tau} + \omega_0^2\int V_c(t')\cdot dt' = \frac{V_T}{R_f} + C_f\frac{dV_T}{dt} - \frac{i}{C}. \tag{12}$$

The first two terms (V_T/R_f and $C_f\,dV_T/dt$) on the right of Eq. (12) represent the contact forces and are, respectively, analogous to elastic and viscous coupling between the ball and the table. When dissipation is present, the time interval of contact π/ω' becomes

$$\frac{\pi}{\omega'} = \frac{\pi}{\omega_0}\left(1 - \frac{1}{(2\tau\omega_0)^2}\right)^{1/2}, \tag{13}$$

where the relaxation time τ is given by

$$\tau = R_2C_2C/C_f. \tag{14}$$

After free fall, the ball maintains contact with the table for half a period π/ω' during which energy is dissipated. Thus the coefficient of restitution may be written from its definition as [4]

$$K \equiv -v_{\text{out}}/v_{\text{in}} = \exp(-\pi/2\tau\omega'). \tag{15}$$

With an appropriate choice of circuit components, and driving frequency, contacts will occur in a short time interval ($\pi/\omega' \ll \pi/\omega$) during which the rectifier conducts. The complete range $0 < K < 1$ is available by varying C_f, which changes nothing else in the analog. The resistance R_f must remain small to simulate instantaneous impacts, a typical assumption necessary to restrict the system to only two control parameters.

After the coefficient of restitution is established, the remaining control parameter α, the ratio of the acceleration due to the vibrating surface and that due to gravity, is derived from the previous equations in a straightforward manner as

$$\alpha = R_2C_2CV_{0T}\omega^2/i. \tag{16}$$

IV. EXPERIMENTAL RESULTS

Many different periodic and chaotic orbits of the ball, as well as the table harmonic oscillation, can be observed on a dual-channel oscilloscope using the dual-channel vertical axis. The sinusoidal traces in the photographs shown in Fig. 3 display voltages corresponding to the table's position in time for four different V_{0T} values. The other traces display voltages $V_b(t)$, corresponding to the parabolic excursions of the ball for $R_f = 2$ kΩ and $C_f = 0.047$ μF. The scope is triggered by the voltage $V_T(t)$. The contacts of the ball with the table correspond to the overlaps of the traces. A simple periodic orbit ($n = 1$) is shown on the top left of Fig. 3. Increasing the table's amplitude causes the bouncing period to double (top right), and double again (bottom left). Further increasing V_{0T} causes chaotic orbits to occur (bottom right). The screen is brightened at a constant table's phase ($\Phi = 3\pi/2$), by connecting to the scope z-axis voltage pulses triggered by V_T. Using this procedure, the student is able to observe the bifurcation diagrams and the Poincaré section of the attractors on screen, as explained below. Bifurcation sequences can easily be observed on the scope either by changing the table amplitude or its frequency on the function generator. These changes correspond to different values of the parameter α, with fixed K. The traces in Fig. 3 were taken on the same frame for quick comparison. By measuring the onset of bifurcation values for the drive voltage amplitude or frequency, the student can estimate the Feigenbaum universal constant.[1] Furthermore, the α values of the first bifurcations for any simple orbit are in close agreement with those predicted from Eq. (4).

In order to determine experimentally the parameter K,

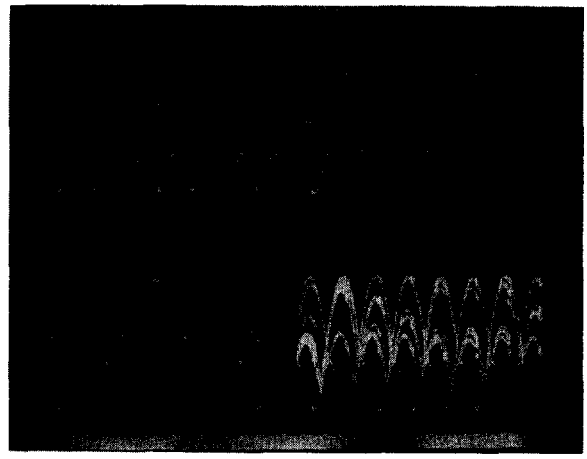

Fig. 3. Oscilloscope dual traces of the bouncing ball simulator showing periodic and chaotic orbits.

one can drive the table with square waves from the function generator. The impulses must have a period that is long compared to the time required for the ball to come to rest on the table. The plot of the impact time versus the impact number follows a geometric progression from which K can be accurately determined.[9] Alternatively, K can be estimated directly either from the ball's velocity or position versus time curves. Figure 4 shows both the position $V_b(t)$ (upper trace) and the velocity—$V_c(t)$ of the ball during one half-period of a square wave $V_T(t)$ for $R_f = 1$ kΩ and $C_f = 0.047$ μF. By measuring the values of the velocity changes during "impacts," which are quantified by the vertical weak lines in the lower trace of Fig. 4, one obtains $K = 0.57 \pm 0.03$ in agreement with the predicted value ($K = 0.6$) derived from Eq. (18) using nominal circuit values. The small kinks observed on the velocity plot at the "impacts" are due to the phase shift caused by C_f. From the upper trace of Fig. 4, $K = (x_{N+1}^{\max}/x_N^{\max})^{1/2} = 0.59 \pm 0.02$, where $x^{\max}$ are the maximum height of the ball for each orbit.

Fig. 4. Oscilloscope traces that simulate the time position $V_b(t)$ (upper trace) and velocity $-V_c(t)$ (lower trace) of the ball bouncing on a fixed table.

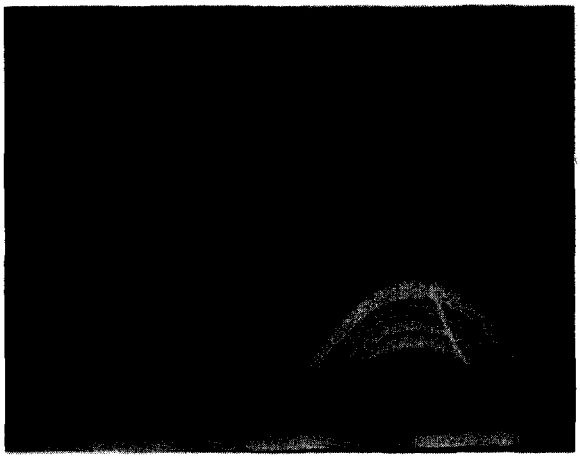

Fig. 5. Oscilloscope traces of the bouncing ball simulator showing the phase space V_b versus—V_c for the same orbits displayed on Fig. 3.

The phase space (ball's velocity versus ball's position) of a large region of the α–K parameter space can be easily observed on the oscilloscope screen, by injecting V_b and V_c as vertical and horizontal deflection voltages, respectively. The phase space for a particular α–K pair is selected from the circuit parameters, and from the driving signal. Figure 5 shows the limiting cycles for a sequence of period one, two, and four followed by chaos for the same four values of α used in Fig. 3, and the same fixed K value. The traces are brightened when the table's phase is $\Phi = 3\pi/2$. In this way, the Poincaré section of each diagram is shown easily, and the strange attractor is superposed on the diagram for the chaotic movement (bottom right). The limiting cycle for period eight, although also observed, is not shown in Fig. 5. Again, all traces are taken on the same frame for quick comparison. These results are in close agreement with those generated by numerical simulation from the parametric recursion relations Eqs. (2) and (3). The small overshoots to the left of each trace shown in Fig. 5 represent the velocity phase shifts during contacts caused by the viscous coupling between the ball and the table.

The Poincaré cross sections in phase space can be observed on the scope by connecting a pulse generator to the z axis. The pulses are triggered by a selected phase Φ of the driving voltage $V_T(t)$. The bright spots on Fig. 5 represent the Poincaré section for $\Phi = 3\pi/2$ for each of the periodic orbits, and for a particular chaotic motion. Reducing the trace brightness on the scope, the student is able to observe only the Poincaré sections of each periodic or chaotic orbit. The Poincaré section of a chaotic orbit is called a strange attractor, i.e., an attractor in the sense that for initial conditions far from it, the representative point (bright spot) of each of the resulting orbits converges to the attractor. Once "in" the attractor, nearby points "strangely" tend to diverge at an exponential rate.[10] These attractors are self-similar over many length scales, and so may be characterized by a noninteger fractal dimension.[10]

Figure 6 shows a strange attractor for $\alpha = 4.5$ and $K = 0.75$ photographed directly from the oscilloscope using a exposure time of 45 s. The horizontal and vertical axes represent the velocity and position of the ball, respectively. Voltage pulses taken at a selected phase of the driving voltage intensify the screen once each table cycle. The complexity of the attractor, created by the overlap of the first families of orbits is revealed by the five leaves that compose the manifold. An expanded view of the far left leaf of the attractor [Fig. 6(b)] illustrates the self-similarity. Further

Fig. 6. Poincaré section (V_b versus $-V_c$) of a strange attractor for $\alpha = 4.5$, $K = 0.75$, and $\Phi = 3\pi/2$. The entire attractor is shown in (a). Expanded views are shown in (b) and (c).

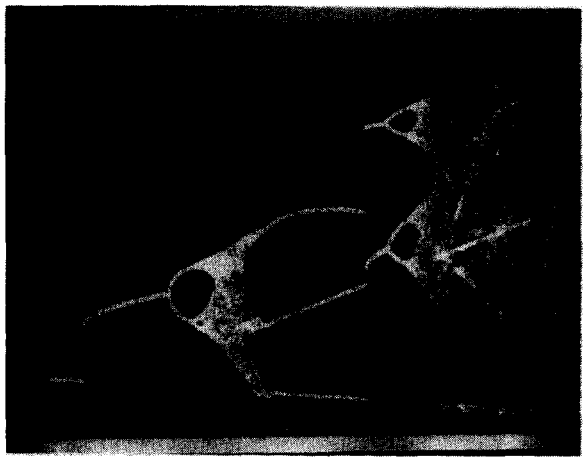

Fig. 7. Bifurcation diagram of the bouncing ball simulator.

expansion of this Poincaré section of phase space [Fig. 6(c)] up to the noise limit shows new layers appearing in a remarkable illustration of a Cantor dust.[10] Again, all these results can be generated from the recursion relations previously derived, Eqs. (1)–(3).

Finally, the bifurcation diagrams for a given K value can be photographed directly from the scope by slowly scanning the amplitude of the driving voltage on the x axis. The other two axes remain the same as before. An open camera collects all the spots during the scanning. The result is shown in Fig. 7 for $K = 0.25$ and $\Phi = 3\pi/2$. The horizontal axis (zero offset) is the normalized table acceleration α. The vertical axis (zero offset) is proportional to the ball's height. The circuit parameters are $R_2 = 10$ kΩ, $C_2 = 0.1$ μF, $C = 0.03$ μF, $R_f = 2$ kΩ, $C_f = 0.1$ μF, $i = 1.47$ μA, and $f = 100$ Hz. The first bifurcation to the left occurs at $\alpha = 2.4$, reasonably close to the value 2.32 predicted by Eq. (4).

V. CONCLUSIONS

An easily constructed electrical analog of the bouncing ball reveals all the characteristics of this well-studied nonlinear system. The table amplitude and frequency, the gravitational force and the position and velocity of the ball are accessible for oscilloscope display for quantitative comparison with numerical analysis based on Newton's equations. Dissipation during the table/ball contact may be quantitatively controlled. In addition, the popular assumption of instantaneous impact may be abandoned. By allowing the table or ball to deform during impact, the student may quantitatively examine collisions with durations shorter or longer than the period of the table, an interesting and easily conceivable physical system described by three parameters. By using the z axis of the oscilloscope, important abstract concepts, such as Poincaré sections and strange attractors, become easily demonstrable. Different configurations of diode feedback in op amp circuits may be used to simulate other interesting nonlinear systems.

ACKNOWLEDGMENT

This work has been supported by the Brazilian agency CNPq.

[1] M. J. Feigenbaum, "Universal behavior in nonlinear systems," Physica 7 D, 16–39 (1983); see also P. Collet and J. P. Eckmann, *Iterated Maps on an Interval as Dynamical Systems* (Birkhauser, Boston, 1980).

[2] R. M. May, "Simple mathematical models with very complicated dynamics," Nature **261**, 459–467 (1976).

[3] E. Fermi, "On the origin of the cosmic radiation," Phys. Rev. **75**, 1169–1174 (1949).

[4] A. B. Pippard, *The Physics of Vibrations* (Cambridge U.P., Cambridge, 1978), Vol. 1, pp. 271–275.

[5] A. Mehta and J. M. Luck, "Novel temporal behavior of a nonlinear system: The complete inelastic bouncing ball," Phys. Rev. Lett. **65**, 393–396 (1990).

[6] S. Celaschi and R. L. Zimmerman, "Evolution of a two-parameter chaotic dynamics from universal attractors," Phys. Lett. A **120**, 447–451 (1987).

[7] N. B. Tufillaro and A. M. Albano, "Chaotic dynamics of a bouncing ball," Am. J. Phys. **54**, 939–944 (1986).

[8] T. M. Mello and N. B. Tufillaro, "Strange attractors of a bouncing ball," Am. J. Phys. **55**, 316–320 (1987).

[9] R. L. Zimmerman and S. Celaschi, "Comment on chaotic dynamics of a bouncing ball," Am. J. Phys. **56**, 1147–1148 (1988).

[10] B. Mandelbrot, *The Fractal Geometry of Nature* (Freeman, New York, 1983).

TENNIS, ANYONE? THE UBIQUITOUS ROLE OF $\sqrt{n}$

In all activities, scientific or otherwise, [Fermi] had a mixture of semi-logical whimsical humor about common-sense points of view. When he played tennis, for instance, if he lost four games to six, he would say: "It does not count because the difference is less than the square root of the sum of the number of games."

S. M. Ulam, *Adventures of a Mathematician* (Scribner's, New York, 1976), p. 164.